Repetitive control-based phase voltage modulation amendment for FOC-based five-phase PMSMs under single-phase open fault

Bing Tian, Li Sun, *Member, IEEE*, Marta Molinas, *Member, IEEE*, and Quntao-An, *Member, IEEE*

***Abstract* — This paper investigates the most elementary phase voltage modulation (PVM) for a more generic Five-phase Permanent Magnet Synchronous Motor (5Ph PMSM) drive under single-phase open fault. Most works on this topic are intended for some specific motor types, and in most cases, it assumes the inverter can still be treated as a linear switching-mode power amplifier. This paper figures out that due to an oscillating neutral the phase voltage is unable to be linearly modulated which is to say the simplest SPWM is problematic to fit a newly developed well-decoupled model under single-phase open fault. To this end, a nonlinear transform incorporating the faulty phase voltage is theoretically proposed which alleviates the influence of oscillating neutral on PVM, and several approaches to cancel the need for phase voltage sensors are comparatively investigated. Accordingly, the PVM with repetitive control and back-EMF compensation is put forward to fix the "faulty inverter" in practice. Plausible PVM approaches are tested experimentally, and the superiority of the proposed PVM is confirmed by experimental results.**

***Index Terms*—phase voltage modulation, oscillating neutral, Five-phase PMSM, single-phase open fault, fault-tolerant control**

I. Introduction

Because of the inherent merits of high-power density reduced torque ripples, and excellent fault-tolerant capacities, the five-phase permanent magnet synchronous motor (5Ph PMSM) has attracted tremendous attention recently[1]. Those salient features are what makes a 5Ph PMSM different from its three-phase counterpart, however, one usually has to make a tradeoff in the motor structural design with respect to a specific application [2]. In some applications, e.g., electric propulsion and electric vehicles, the high-power density shall be primarily guaranteed because the motor drive is supposed to work in a very compact environment. In this regard, the motor tends to have a trapezoidal Back-EMF and/or extra reluctance torque to increase torque production. While in other safe crucial applications, the fault-tolerant capacities are appreciated. In these applications, the motor is subject to a modular design and presents low mutual inductances between phases for the sake of magnetic and thermal isolation [3]. The latter type of motor is usually termed a fault-tolerant motor (FTM) in the literature [4-9]. Apart from the motor structural design, the fault-tolerant performance of 5Ph drives can be further enhanced from the aspect of the software, i.e., fault-tolerant control (FTC). The short circuit and open circuit are the most common types of failures in a motor drive. The short circuit can lead to motor overheating and cause irreversible secondary damage to the rotor's magnet, and thus, this fault type is always transformed to the open fault at its earliest occurrence [10, 11]. In general, the research of open FTC is more significant taking into account the variable failure scenarios. Accordingly, the FTC can be primarily accomplished by the re-configuration of the remaining phase currents. For instance, by re-arranging the remaining phases currents to form an identical Magnetomotive Force (MMF) as before the fault, the motor can still operate steadily. Since the motor is with one or more phases unenergized, some performances, such as the torque and power rating, are inevitably downgraded. Considerable articles have been presented on this topic of how to reduce torque ripples. However, the methods can be quite different between an FTM and a more generalized 5Ph PMSM. Normally, FTC is much easier on an FTM typically with, e.g., a low mutual-inductance, a constant self-inductance or a sinusoidal back-EMF. This is because the constant self-inductance gets rid of rotor position, which implies the coordinate transform in fault mode doesn't have to be specially re-designed since the inductances are always constant under an arbitrarily linear coordinate frame. In contrast, the latter motor type is more complex in fault-tolerant modeling such that the optimal current solution for torque ripple-free can be quite involved, depending on how well the referenced model is decoupled from the rotor position.

The optimal current solution indicates the expected currents of a faulty motor for the purposes of, for instance, minimum torque ripples, minimum Joule Losses (MJL), the equal amplitude of the remaining phase currents. To ensure that the actual motor currents can follow the predefined trajectories or optimal current solutions, phase-voltage modulation (PVM) also require investigation. The PVM is most elementary in an inverter-driven system, however, the improper implementation could lead to a false current in fault mode. The 5Ph PMSM gets severely unbalanced in the event of open-fault, and the classical sinusoidal-PWM (i.e., SPWM, and the SVPWM is regarded as a special case of SPWM) typically for a balanced system, is likely inapplicable for a faulty motor drive. In other words, the neutral point of a faulty motor drive is severely affected by the faulty phases, and thus the PVM may be not as simple as it

seems in a balanced drive. The oscillating neutral in fault mode is somehow ignored in the early literature probably due to no available FOC techniques formerly. Thereby in most articles, the hysteresis current controller is utilized to track the AC references. However, the hysteresis controller may be undesirable in industrial applications due to the inconstant switching frequency as well as the large current ripple that is associated with the calculation frequency.

The FTC is mostly conducted on FTMs where torque ripple reduction is evaluated. For instance, A. Mohammadpour, [3], develops a global closed-form optimum algorithm to produce ripple-free torque. In [5], a genetic algorithm is proposed to solve the torque-free currents for a flux-switching motor having a small mutual-inductance, and a hysteresis current controller is employed. It must be noticed that the above methods are quite parameter-dependent such that the optimal current solution, which is usually solved offline, sometimes may fail in the real drive. As concluded in [3], the ideal torque-ripple free is sometimes unachievable in practice, and this is perhaps due to the fact that the real FTM drive is more complex than the theoretical one. To avoid hysteresis control, Guohai Liu, [12], comparatively studied two SVPWM strategies for an FTM under a single-phase open fault. However, the oscillating neutral due to open fault is somehow ignored, and the applications of the presented SVPWM is only tested at a low speed where the oscillating neutral is not severe. Qian Chen, [13], developed an asymmetrical SVWPM for an FTM drive under open fault conditions. However, the oscillating neutral on PWM implementation is still incorporated. Hugo Guzman, [4], firstly proposed a field-oriented control (FOC) method for a five-phase induction motor under a single-phase open fault where the remaining phase back-EMFs can be decoupled from rotor position under the presented new d-q frame. Huawei Zhou, [6], proposed a remedial FOC for an FTM where neutral voltage pulsation is reported to be negligible. However, this method is only tested on the permanent magnet motor with constant self-inductances and low mutual inductances. Motivated by the work of [4], B. Tian, [14], comes up with a decoupled model for a more generic 5Ph PMSM under a single-phase open fault. Within this model, the inductances and rotor flux under the new d-q frame are DCs which means d-q frame PI controls can be applicable. Unfortunately, the authors fail to demonstrate how the PVM is performed in the presence of an oscillating neutral. Luming Chen, [15], presents a post-fault decoupling vector control for a 5Ph FTM under a single-phase open circuit. Except for the fact that the parameters of the presented model are time-variant, it is also incapable to document the possibility of the motor working towards a much high speed where the neutral is supposed to oscillate more severely. In [16], the optimal current under the constraint of maximum reluctance torque is attempted to drive a 5Ph PM assisted synchronous reluctance motor (PMa-SynRm). Through a desirable performance is reported to be achieved, it remains unknown on how to offset the oscillating neutral. [17] presents a virtual vector-based direct-torque-control (DTC) for a 5Ph induction motor under open faults as the extension of the work [4], but it is still uncertain how to cope with the oscillating neutral when implementing voltage space vector synthesis. In [18], a sliding mode control is employed to regulate the d-q frame current which is believed to able to suppress unmodelled oscillating neutral under low speeds. In the recent works of [7] and [8], model predictive control and torque-ripple reduction through the third harmonic injection, are, respectively, attempted by overlooking the oscillating neutral unconsciously. Li Zhang, [19], revisits the oscillating neutral issue in the implementation of the SVPWM-based DTC for a 5Ph FTM under single-phase open fault. However, the oscillating neutral compensation is performed basing on the FOC intended for the healthy mode which possesses 4 controllable degrees of freedom (DOFs), besides, the mutual inductances are also neglected. Even though more and more advanced controls, rather than hysteresis control, are reported for 5Ph PMSMs under open faults, their applications are restricted to either a specified motor type or the ill-considered oscillating neutral. To the author's knowledge, FOC is still appealing in the industry since the faulty motor can be operated with d-q frame PI controllers under PWM techniques, and it is also less parameter-dependent than the model-based methods [20]. The successful FOC of faulty motor drives relies on a well-decoupled model which has been established recently [14], but the PVM, which seems fairly straightforward in a balanced system, still lacks a solid foundation due to the ill-consideration of the oscillating neutral (particularly the one originating from open faults).

This paper is built on the fault-tolerant decoupled model in [14] which benefits from having a constant L_d, L_q, e_d, and e_q under a new coordinate frame, and this work aims at the most basic PVM issue for a more generic 5Ph PMSM under single-phase open fault. As aforementioned, the neutral point of a faulty drive is oscillating due to open faults, and thus the PVM, in this case, is not that straightforward as it seems in a balanced drive. In light of this, a nonlinear transform incorporating the faulty phase voltage is theoretically proposed to improve the fault-tolerant FOC. However, in many applications the phase voltage sensing techniques are unavailable. To tackle this, several feasible approaches are comparatively investigated and the PVM combining repetitive controls and back-EMF compensation is put forward. Contrast experiments are also provided to validate the effectiveness of the proposed method.

The major issue addressed in this paper can be understood like this: the inverter is not a "linear switching-mode power amplifier" any longer in fault mode, and thus special handling in PVM is required. The novelties of this work can be classified as the followings: 1) a nonlinear transform incorporating the faulty phase voltage is theoretically proposed to fix the PVM under an oscillating neutral, and 2) a repetitive controller joint with the faulty phase back-EMF compensation is put forward in practice which removes the need for phase-voltage sensors. Additionally, the potential significance of this paper is: the proposed method also forms a basis for some more advanced techniques, e.g., DTC and model predictive control, since both techniques are adapted from the basic FOC methodology. Meanwhile, the limitation of the proposed method can be

summarized as: 1) the common-mode voltage (CMV), which is originating from switching activities, is currently unable to be reduced yet; and 2) the proposed method only suits a star-connected 5Ph PMSM fed by a five-phase half-bridge inverter.

II. Decoupled Model and Unsolved Problem

A. The previous decoupled model

The investigated motor type is a star-connected 5Ph PMSM which is fed by a typical five-phase half-bridge IGBT-based inverter. Without losing generality, assume phase-A is open-circuited. The decoupled model and torque representations for the case of a motor under a single-phase open fault are given by (1) and (2) [14]. The controllable DOFs of a 5Ph drive in fault mode downgrade to 3 which can be decomposed into one 2-D plane for fundamental frequency control and a half 2-D plane for 3rd harmonic control. In (1) and (2), u_d, u_q, u_{q3} are voltages of d-q-q_3 frame; i_d, i_q, i_{q3} are currents of d-q-q_3 frame; ω, θ are, respectively, the rotor speed and position; p is the pole-pair; ψ_{m1} and ψ_{m3} are, respectively, the magnitudes of 1st and 3rd magnetic fluxes; and L_d, L_q, L_{q3} are, respectively, d-, q- and q_3-axis inductances, which are now DCs under d-q-q_3 frame. The crucial Clarke and Park matrices for the decoupled modeling are, respectively, given by

$$\left[\mathbf{T}_{\text{Park}}\right]=\begin{bmatrix}\cos\theta & \sin\theta & 0 & 0\\ -\sin\theta & \cos\theta & 0 & 0\\ 0 & 0 & 1 & 0\\ 0 & 0 & 0 & 1\end{bmatrix} \tag{3}$$

$$\left[\mathbf{T}_{\text{Clarke}}\right]=\frac{2}{5}\begin{bmatrix}\cos\delta-1 & \cos2\delta-1 & \cos3\delta-1 & \cos4\delta-1\\ \sin\delta & \sin2\delta & \sin3\delta & \sin4\delta\\ \sin3\delta & \sin6\delta & \sin9\delta & \sin12\delta\\ 1 & 1 & 1 & 1\end{bmatrix} \tag{4}$$

Where δ denotes the motor spatial angular displacement between adjacent phases, with $\delta=2\pi/5$; and $[\mathbf{T}_{\mathbf{Park}}]$ and $[\mathbf{T}_{\mathbf{Clarke}}]$ indicates, respectively, Park and Clarke matrices, where the last row corresponds to the zero-sequence transformation. With the above matrices, this AC faulty motor can be transformed into a DC model, however, this does not suggest that the PVM can be easily applied. Since the faulty drive comprises not only a faulty motor but also a faulty inverter, the faulty inverter is still unmodeled yet. In this paper, it is figured out that the absence of an effective PVM for this decoupled model is due to the severe neutral oscillation as shown in Fig.1.

Under single-phase open fault, the neutral point (indicated as "N") voltage is drifting over the mid-point of the capacitor bank (indicated as "O"). Normally, the inverter works by the direct modulation of pole voltages, i.e., v_{AO}, v_{BO}, v_{CO}, v_{DO}, v_{EO}, where phase voltages, i.e., v_{AN}, v_{BN}, v_{CN}, v_{DN}, v_{EN} are only co-products. Obviously, under a single-phase open circuit, it produces a false phase voltage because of oscillating neutral.

Fig.1 reveals the FOC-based FTC of a 5Ph drive in the previous article where the oscillating neutral is not incorporated during the decoupled modeling (or rather, the faulty inverter is still unmodelled yet). Overlooking the oscillating neutral in PVM can lead to an unexpected phase voltage/current and thus this problem should be dealt with carefully. Intuitively the oscillating neutral is intimately related to the open-circuited phase back-EMF, but up to present, it still lacks a solid foundation on how to weaken the influence of oscillating neutral on PVM with the back-EMF information. Thus, the overriding goal of this paper is to explore how to generate the expected phase voltage correctly through PVM.

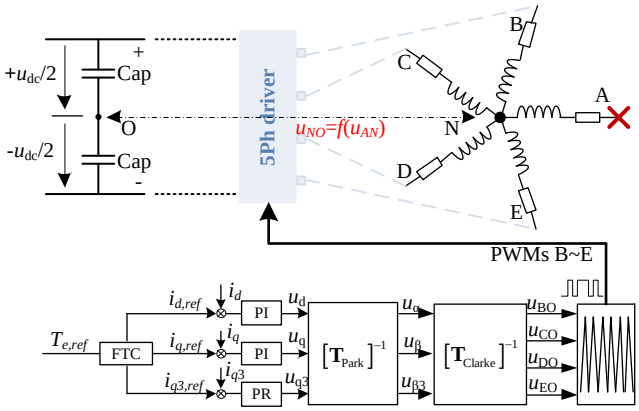

Fig.1 The block diagram of FOC-based FTC in the previous literature where the oscillating neutral is somehow neglected during the SPWM implementation.

In Fig.1, $T_{e,ref}$ represents the torque command which is assigned by a speed PI controller; and the high-level FTC stands for some constraints (e.g., minimum joule losses or/and minimum torque ripples) to re-configure the motor currents under d-q-q_3 frame. Readers may refer to the appendix for the optimal current solution under the constraint of minimum torque ripples. Also notice that the d-q-q_3 frame feedforward terms $-\omega L_q i_q$, $\omega L_d i_d$ and $\omega\psi_{m1}$ as well as $3\psi_{m3}\cos(3\theta)$ are neglected for the moment in Fig.1. Numerous articles have been published on FTC, but how to generate the expected voltage correctly via inverter chopping under an oscillating neutral is still missing for this decoupled model and this constitutes the major contribution of this paper.

B. Unsolved problem

$$\begin{bmatrix}u_d\\ u_q\\ u_{q3}\end{bmatrix}=R_s\begin{bmatrix}i_d\\ i_q\\ i_{q3}\end{bmatrix}+\begin{bmatrix}L_d & 0 & 0\\ 0 & L_q & 0\\ 0 & 0 & L_{q3}\end{bmatrix}\frac{d}{dt}\begin{bmatrix}i_d\\ i_q\\ i_{q3}\end{bmatrix}-\omega\begin{bmatrix}0 & L_q & 0\\ -L_d & 0 & 0\\ 0 & 0 & 0\end{bmatrix}\begin{bmatrix}i_d\\ i_q\\ i_{q3}\end{bmatrix}+\omega\begin{bmatrix}0\\ \psi_{m1}\\ 3\psi_{m3}\cos3\theta\end{bmatrix} \tag{1}$$

$$T_e=\frac{5p}{2}\left[i_d i_q(L_d-L_q)+i_q\psi_{m1}\right]+\frac{5p\psi_{m3}}{2}\left[3i_{q3}+\frac{3(i_d\sin2\theta+i_d\sin4\theta-i_q\cos2\theta+i_q\cos4\theta)}{2}\right] \tag{2}$$

III. PVM INVESTIGATION

A. The oscillating neutral issue due to open faults

From the control viewpoint, the 5Ph drive in fault mode can be the equivalent of a 4Ph drive, considering there is no power supply to the faulty phase. Nevertheless, the following points about this faulty 5Ph drive still hold [19, 21]

$$u_{XN} = u_{XO} - u_{NO},\ X = A,B,C,D,E \tag{5}$$

$$u_{XO} = s_X u_{dc} - 0.5u_{dc},\ X = B,C,D,E \tag{6}$$

$$u_{AN} + u_{BN} + u_{CN} + u_{DN} + u_{EN} \equiv 0 \tag{7}$$

Where u_{XN} indicates the phase-to-neutral voltage, with X=A,B,C,D,E; u_{XO} are the pole voltages measured between the motor terminal and 'O' point; u_{NO} is neutral to 'O' point voltage, and u_{dc} is the DC link voltage.

Substituting (5) and (6) into (7) yields

$$u_{NO} = \underbrace{\frac{u_{dc}}{4}\left(s_B + s_C + s_D + s_E\right) - \frac{u_{dc}}{2}}_{\text{CMV}} + \frac{1}{4}u_{AN} \tag{8}$$

From (8), the neutral potential is oscillating when the motor is spinning. For the convenience of analysis, u_{NO} is divided into two parts: 1) CMV and 2) ¼uAN. The CMV is due to the switching activity of power devices, which implies CMV is difficult to be fully removed in an inverter-driven system. From (8), the CMV evidently oscillates at the switching frequency, which means its impact on phase currents can be weakened by the winding impedance. According to some literature, the CMV can be reduced by a modified SVPWM, however, as indicated in [22, 23] that the reduction of CMV is, somehow, achieved at the cost of higher current distortion. Given this, this paper is conservative with respect to the CMV reduction by advanced SVPWMs. Unlike the CMV effect, the oscillating neutral caused by open faults is at the fundamental frequency and unlikely to be damped by the stator impedance which eventually leads to severe current oscillation. Thus, this work is constructed to enhance voltage and/or current controllability by addressing the oscillating neutral which is hereinafter defined as the one originating from open faults.

B. The theoretical solution proposed to the oscillating neutral

According to the decoupled model, the expected phase voltages can be derived by the following representation.

$$\left[u_{BN}, u_{CN}, u_{DN}, u_{EN}\right]^{\mathrm{T}} = \left[\mathbf{T}_{\mathrm{Clarke}}\right]^{-1}\left[u_\alpha, u_\beta, u_{\beta 3}, u_{\mathrm{o}}\right]^{\mathrm{T}} \tag{9}$$

Where u_α, u_β are the assigned reference voltages of the α-β frame; $u_{\beta 3}$ is the assigned reference voltage of β_3-axis; and u_o is the zero-sequence voltage, which is responsible for the zero-sequence current. By using "expected phase voltages," it means they are the very desired phase voltages for the FOC, yet one probably obtains a false phase voltage when modulating the pole voltage references because of the oscillating neutral. This result implies that modification is necessary on the pole voltage references to obtain the correct "expected phase voltages."

Substituting (5) and (8) into (9), one can obtain the following equation revealing the relationship between α-β frame voltages, pole voltages, and the open phase voltage.

$$\left[u_\alpha, u_\beta, u_{\beta 3}, u_{\mathrm{o}}\right]^{\mathrm{T}} = \left[T_{\mathrm{Scale}}\right]\left[u_{\mathrm{BO}}, u_{\mathrm{CO}}, u_{\mathrm{DO}}, u_{\mathrm{EO}}\right]^{\mathrm{T}} + \left[0.5u_{\mathrm{AN}}, 0, 0, -4u_{\mathrm{o}}\right]^{\mathrm{T}} \tag{10}$$

$$\left[T_{\mathrm{Scale}}\right] = \frac{2}{5}\begin{bmatrix} \cos\delta + \frac{1}{4} & \cos 2\delta + \frac{1}{4} & \cos 3\delta + \frac{1}{4} & \cos 4\delta + \frac{1}{4} \\ \sin\delta & \sin 2\delta & \sin 3\delta & \sin 4\delta \\ \sin 3\delta & \sin 6\delta & \sin 9\delta & \sin 12\delta \\ 1 & 1 & 1 & 1 \end{bmatrix} \tag{11}$$

Where the [**T**$_{\mathbf{Scale}}$] denotes the scaling transformation matrix and the second vector accounts for the oscillating neutral. From (9), the existence of u_{AN} is noticeable, and this explains why the most common SPWM technique, which works for a balanced system, always fails under fault conditions. In fact, the phase voltage is the sum of pole voltages and neutral voltage. However, it is the pole voltage that matters in generating the "expected phase voltage". To exclude the neutral voltage related term, define:

$$\left[u_{\mathrm{BO}}, u_{\mathrm{CO}}, u_{\mathrm{DO}}, u_{\mathrm{EO}}\right]^{\mathrm{T}} = \left[T_{\mathrm{Scale}}\right]^{-1}\left[v_x, v_y, v_z, v_{\mathrm{o}}\right]^{\mathrm{T}} \tag{12}$$

$$\left[v_x, v_y, v_z, v_{\mathrm{o}}\right]^{\mathrm{T}} = \left[u_\alpha, u_\beta, u_{\beta 3}, u_{\mathrm{o}}\right]^{\mathrm{T}} - \left[0.5u_{AN}, 0, 0, -4u_{\mathrm{o}}\right]^{\mathrm{T}} \tag{13}$$

Where v_x, v_y,v_z, v_o are the assigned references of x-y-z-o frame. The benefit of having a new coordinate is that the pole voltage can be straightforward if x-y-z-o frame references are accessible. For simplicity, v_o is set to 0 in order to generate pole voltages with a zero-sum. It can be easily extrapolated that the zero-sequence voltage is $4u_{\mathrm{NO}}$ in this case. In fact, v_{o} is responsible for the zero-sequence current regulation; however, it is of no use for a star-connected motor, and thus v_{o} is fixed to zero. Finally, one can obtain the following nonlinear transformation.

$$\begin{aligned} &\left[u_{\mathrm{BO}}, u_{\mathrm{CO}}, u_{\mathrm{DO}}, u_{\mathrm{EO}}\right]^{\mathrm{T}} \\ &= \left[T_{\mathrm{Scale}}\right]^{-1}\left(\left[u_\alpha, u_\beta, u_{\beta 3}, u_{\mathrm{o}}\right]^{\mathrm{T}} - \left[0.5u_{AN}, 0, 0, -4u_{\mathrm{o}}\right]^{\mathrm{T}}\right) \end{aligned} \tag{14}$$

The equation (14), which is calculated in every control cycle in a DSP (Digital signal processor), is the proposed approach to sort out the oscillating neutral. This nonlinear transform can be illustrated by the blue blocks of Fig.2. Unlike the SPWM for a balanced system, $[\mathrm{T}_{\mathrm{Scale}}]^{-1}$, instead of $[\mathrm{T}_{\mathrm{Clarke}}]^{-1}$, is hereinafter employed to derive the desired pole voltages, and simultaneously the faulty phase voltage compensation is performed onto the α-axis. This compensation is dependent on the re-construction of open circuited phase voltage, and thus (14) is termed "a nonlinear transform". With this nonlinear transform, it is possible to generate the "expected phase voltage" via modulating pole voltages. Accordingly, the most simple and effective PVM can be represented by the blue blocks of Fig.2, and this is also the most straightforward solution to the problem of the oscillating neutral. Notice that only the pole voltages are re-defined, and the Clarke transform used in the upper-level FOC is kept unchanged.

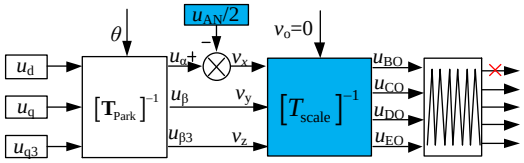

Fig.2 The block diagram of proposed PVM where the influence of oscillating neutral can be theoretically weakened with u_{AN}.

C. Possible solutions regarding most 5Ph drives

As analysis previously, the oscillating neutral severely affects PVM which further induces uncontrollable phase currents. Since the PVM is most elementary in an inverter-driven system, its effectiveness shall be firstly guaranteed such that the higher-level FTC, e.g., torque ripple reduction, can be applied. The readers refer to the appendix for the optimal current solution for torque ripple-free purpose, however, this is not the focus of this paper. Several approaches are presented in this paper to weaken the influence of the oscillating neutral on PVM. It should also be noticed that the oscillating neutral which is originating from open faults cannot be eliminated physically, and we merely concentrate on how to weaken its influence on PVM.

Method I: Conventional SPWM for a balanced system

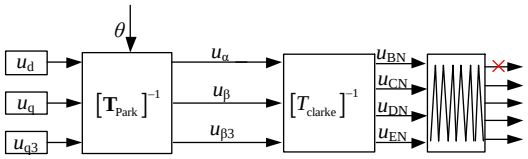

Fig.3 The block diagram of SPWM typically for a balanced system.

Fig.3 refers to the SPWM which is most popular for a balanced system. This SPWM uses the Park and Clarke matrices intended for the decoupled modeling and believes the phase voltage is identical to the pole voltage. However, this is not the case with respect to the faulty motor with an oscillating neutral. As the SVPWM can be regarded as one special case of the SPWM technique, it is safe to conclude SVPWMs will not work properly if the SPWM fails firstly. Thereby, only the SPWM is carried out experimentally.

Method II: the SPWM combining back-EMF compensation

From Fig.2, it is evident that u_{AN} is crucial for the correct PVM. However, the sampling of u_{AN} is not easy in most industrial applications, and this can be convinced by the fact: the faulty phase voltage is PWM alike even though the faulty winding has been isolated from the power converter. Under the open circuit fault, u_{AN} can be represented by

$$u_{\mathrm{AN}} = \frac{d}{dt}\left(L_{\mathrm{AB}}i_{\mathrm{B}} + L_{\mathrm{AC}}i_{\mathrm{C}} + L_{\mathrm{AD}}i_{\mathrm{D}} + L_{\mathrm{AE}}i_{\mathrm{E}}\right) + e_{\mathrm{A}} \tag{15}$$

As can be seen, u_{AN} comprises not only the Back-EMF constituent but also the noisy mutual-induced EMFs, which are also PWM signals. The inclusion of voltage sensors increases the system volume as well as the capital expenditure and thus they are typically avoided. Thereby, a soundest approach with sufficient robustness is to resort to the back-EMF, and this can be graphically illustrated by Fig.4.

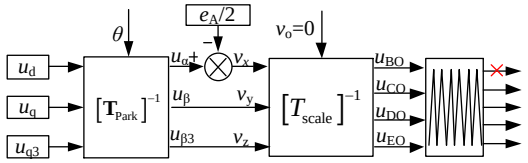

Fig.4 The block diagram of SPWM combining back-EMF compensation.

In Fig.4, the proposed $[T_{Scale}]^{-1}$, rather than the commonly adopted $[T_{Clarke}]$, is utilized to fix the "faulty inverter". It must be noticed that the $[T_{Clarke}]$ used in the upper-level FOC is kept unchanged. This method can be quite efficient with respect to an FTM which pursues quite low mutual inductances. u_{AN} can be reconstructed by the following formula by neglecting mutual inductances

$$u_{\mathrm{AN}} \approx e_{\mathrm{A}} \approx -\omega\psi_{\mathrm{m1}}\sin\theta - 3\omega\psi_{\mathrm{m3}}\sin 3\theta \tag{16}$$

However, regarding a more generic 5Ph PMSM, the mutual inductances are non-negligible, and considerable mutually induced EMFs can be easily re-coupled onto the open-circuited winding. The mutually induced EMF can be represented by:

$$u_{MEMF} = \frac{d}{dt}\left(L_{\mathrm{AB}}i_{\mathrm{B}} + L_{\mathrm{AC}}i_{\mathrm{C}} + L_{\mathrm{AD}}i_{\mathrm{D}} + L_{\mathrm{AE}}i_{\mathrm{E}}\right) \tag{17}$$

Where u_{MEMF} indicates the mutually induced EMF; and the mutual inductances can be approximated by:

$$\begin{aligned} L_{\mathrm{AB}} &\approx M_{AB} + \Delta M_{\mathrm{AB}}\cos(2\theta + 1.6\pi) \\ L_{\mathrm{AC}} &\approx M_{AC} + \Delta M_{AC}\cos(2\theta - 0.8\pi) \\ L_{\mathrm{AD}} &\approx M_{AD} + \Delta M_{AD}\cos(2\theta + 0.8\pi) \\ L_{\mathrm{AE}} &\approx M_{AE} + \Delta M_{AE}\cos(2\theta - 0.8\pi) \end{aligned} \tag{18}$$

Where M_{AB}, M_{AC}, M_{AD}, M_{AE} are the constant constituents of mutual inductances, and ΔM_{AB}, ΔM_{AC}, ΔM_{AD}, ΔM_{AE} are the alternating constituents. As per (17), the magnitude of u_{MEMF} can be scaled by the motor speed. At high speeds, the mutually induced EMF is so significant that this approach may probably fail. In short, the method is efficient only at the mid-low speed for the studied motor type in this paper.

Method III: The SPWM considering the repetitive control

The faulty phase voltage, u_{AN}, can be treated as a feedforward if it is projected into the d-q frame. This result implies that the compensation can be replaced by the incorporation of some closed-loop controllers, for instance, repetitive controller, as shown in Fig.5. As the mutually induced EMF is quite complex in modeling, it is temporarily ignored for simplification. Then transforming the back-EMF (which is calculated up to 3rd harmonics) to the d-q frame with the inverse Clarke yields:

$$\begin{aligned} u_{\mathrm{d,Fw}}\big|_{u_{MEMF}=0} &= -0.5e_{\mathrm{A}}\cos\theta \\ &\approx -0.25\omega(\psi_{\mathrm{m1}} + 3\psi_{\mathrm{m3}})\sin 2\theta - 0.75\omega\psi_{\mathrm{m3}}\sin 4\theta \end{aligned} \tag{19}$$

$$\begin{aligned} u_{\mathrm{q,Fw}}\big|_{u_{MEMF}=0} &= -0.5e_{\mathrm{A}}\sin\theta \\ &\approx -0.25\omega\psi_{\mathrm{m1}} + 0.25\omega(3\psi_{\mathrm{m3}} - \psi_{\mathrm{m1}})\cos 2\theta + 0.75\omega\psi_{\mathrm{m3}}\cos 4\theta \end{aligned} \tag{20}$$

Where $u_{d,Fw}$, and $u_{q,Fw}$ are the equivalent feedforward voltages under the d-q frame which fluctuate at two and four times the synchronous speed. It is important to emphasize that the mutually induced EMF is also composed of the 1st and 3rd harmonics provided the control of i_q=constant is adopted. These mutually induced EMFs likewise oscillate at even frequencies when projecting them into d-q frame.

Overall, these oscillating feedforwards can be removed by adopting d-q frame repetitive controllers. Notice that the PI plus RC scheme is also employed to regulate the q_3-axis 3rd harmonic current as per (1).

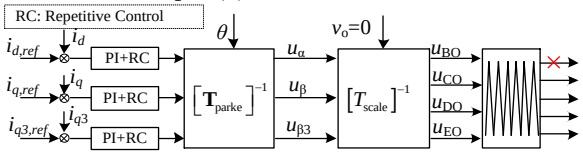

Fig.5 The unitization of a repetitive control to replace the faulty-phase voltage compensation.

The repetitive control is an important method to eliminate steady-state harmonics with multiple frequencies and has been

successfully employed in the applications of harmonic rejection and positioning control of 3Ph systems [24, 25]. The digital implementation of RC can be illustrated in Fig.6.

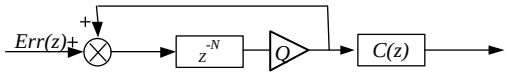

Fig.6 The block diagram of repetitive control.

In Fig.6, Q is the forgetting factor which is responsible for the RC bandwidth; N corresponds to the number of sampling points per fundamental period of the repeatable disturbances, and $C(z)$ represents the amplitude and/or phase corrections. Notice that a phase-lead correction is required to offset the digital delays. The repetitive control can be regarded as a series of resonant controllers working in parallel, however, it consumes only one multiplication per sampling period and thus is quite suitable for this scenario.

Nevertheless, the performance of this closed-loop method is still unsatisfactory at high speeds. This can be convinced by the fact: at high speeds, u_{AN} is so large that the bandwidth of RC shall be quite narrow to provide sufficient control gain, however, this could easily lead the system into the unstable margin. Thus, in practice, Q is adjusted to a decent value which allows enough stability margin. This means the harmonic currents caused by the increasingly significant back-EMF and mutually induced EMFs are difficult to be fully suppressed.

Method IV: The proposed PVM combining repetitive controls and back-EMF compensation

In consideration of the above deficiencies of RC at high speeds, a combination of RCs and Back-EMF compensation is proposed in this paper, and it can be illustrated by Fig.7. The open-loop back-EMF compensation is fast and stable, and it alleviates the need for large control gains for RC at high speeds and thus improves system stability margin without losing the attenuation abilities to mutually induced EMF disturbances.

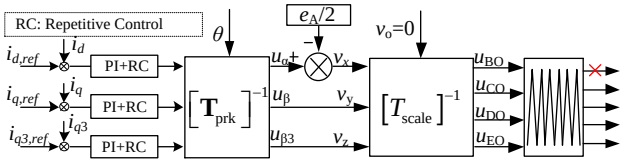

Fig.7 The proposed PVM which combines repetitive controls and back-EMF compensation.

The reconstruction of e_A depends on motor parameters ψ_{m1} and ψ_{m3} which are the most easily accessible motor parameters, and the unmodelled mutual-induced EMF can be identified by the repetitive controllers. Thereby, this composite approach is more practical to offset the influence of the oscillating neutral.

IV. RC PREFERENCES AND OPERATING LIMITS

A. RC preferences

The ideal RC is quite aggressive and thus a modified RC is suggested in numerous articles that can be graphically represented by Fig.6. In Fig.6, a forget factor Q, which is within the set (0,1], is introduced. By reducing Q, the bandwidth of RC has the potential to be widened with, however, a lowered resonance peak. The transfer function of this RC in the discrete-time domain is given by:

$$G_{RC}(z) = C(z)\frac{Qz^{-N}}{1-Qz^{-N}},\ C(z) = K_{rc}z^{m} \tag{21}$$

Where k_{rc} stands for the control gain, z^m represents a phase lead correction that advances the RC output by m sampling periods.

The primary concern in the implementation of RCs is how to select N. In this adjustable speed drive, an angular-based RC is adopted whose effectiveness has been justified in the previous articles[24, 25]. In the angular based RC, the critical parameter N is derived from the cyclic rotor position. Since the repeatable disturbances are even-order harmonics, N can be selected by

$$N = floor(\frac{100}{n}2\theta), n = 1,2,3,4,5,\cdots \tag{22}$$

Where 2θ represents the lowest frequency among these repeatable disturbances with θ being mapped between 0 and 2π; n is a divisor which determines the memory array size, and N is truncated to the nearest integer. Given the available memory size of the adopted DSP, N is fixed to 157 which means 157-word size is required to implement each RC.

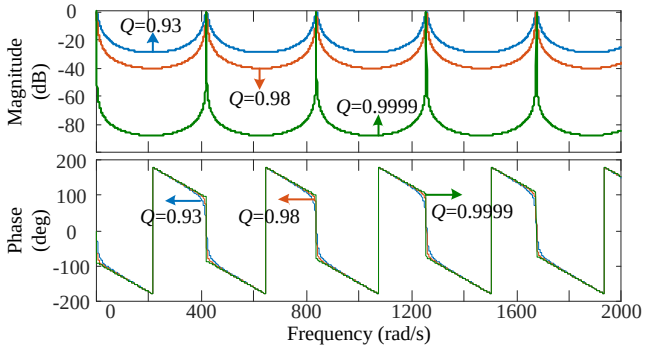

Fig.8 Bode plots of RCs under different forgetting factors.

Bode plots of RCs under different forgetting factors are plotted with the resonance peaks being normalized. From Fig.8, a lower Q always contributes to widening the bandwidth of RC. The criterion for selecting Q can be referred to [26], where the RC is treated as numerous quasi-resonant controllers in parallel. The speed variation is within 1.79 rad/s (electrical) according to the test, and this means the bandwidth of RC shall double this frequency in order to kill the even-order harmonics. Given this, Q is supposed to be 0.948 under 1000 rpm. However, the RC is also prone to non-repeatable disturbances, such as measurement noises and a step command. These disturbances are then recorded in the RC's memory if not damped timely. To damp non-repeatable disturbances quickly, a lower Q is always preferred which prevents the RC output from undergoing unbounded. Thus, in this adjustable speed motor drive, Q is further adjusted according to the "trial and error" method which is eventually fixed to 0.93. The q_3-axis RC shares a similar design procedure and is not detailed herein.

B. Permissible operation range

In order to analysis the feasible control region, suppose the faulty motor is driven to a certain speed under a constant i_q. According to (1), the demanded d- and q_3- axis voltages (at steady state) can be formulated as:

$$u_{d,ref} = -\omega L_q i_q,\ u_{q3,ref} = 3\omega\psi_{m3}\cos(3\theta) \tag{23}$$

Where $u_{d,ref}$, $u_{q3,ref}$ are, respectively, the demanded d- and q3-

axis voltages to zero i_d and i_{q3}. Then, convert the d-q-q_3 frame voltages to the phase coordinate frame under the proposed nonlinear transform, one can have the following relationship

$$\begin{aligned} u_{BO,ref} &= f_{BO}(u_{q,ref},\omega,i_q,u_{AN}) \le 0.5u_{dc} \\ u_{CO,ref} &= f_{CO}(u_{q,ref},\omega,i_q,u_{AN}) \le 0.5u_{dc} \\ u_{DO,ref} &= f_{DO}(u_{q,ref},\omega,i_q,u_{AN}) \le 0.5u_{dc} \\ u_{EO,ref} &= f_{EO}(u_{q,ref},\omega,i_q,u_{AN}) \le 0.5u_{dc} \end{aligned} \quad (24)$$

Where $u_{BO,ref}$, $u_{CO,ref}$, $u_{DO,ref}$, $u_{EO,ref}$ represent the demanded pole-voltages which have been re-defined with the proposed nonlinear transform. Notice that the pole voltages shown in (24) is supposed to be less than $0.5u_{dc}$, otherwise pole voltages will be overmodulated. The detailed expressions of pole voltage references are so complex that they are not being presented in this work. However, it is easy to deduce that pole voltages are functions of the variables: $u_{q,ref}$, ω, u_{AN}, and i_q (which is associated with load condition). Currently, it is difficult to work out an analytical solution that discloses the feasible operation range of this faulty motor drive. However, aided with the powerful MATLAB software, a plot regarding the available $u_{q,ref}$ over motor speeds can be presented which is referred to as $u_{q,max1}$ in Fig.9. Meanwhile, the available $u_{q,ref}$ under the previous Clarke and Park transforms is also plotted, which is termed $u_{q,max0}$ in Fig.9.

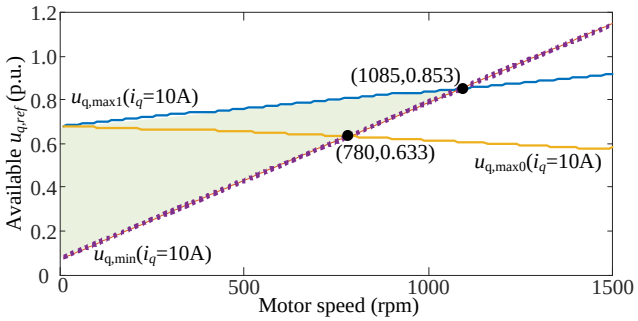

Fig.9 Linear modulation region of pole voltages under a heavy load.

Fig.9 reveals the linear modulation region of pole voltages under a heavy load. In this figure, $u_{q,ref}$ has been normalized with respect to $0.5u_{dc}$, and the preference of $u_{q,ref}$ larger than $u_{q,max1}$ (or $u_{q,max0}$) is subject to the overmodulation of pole voltages. As evident in Fig.9, the permissible range of $u_{q,ref}$ is much wider after the proposed neutral voltage compensation. On the other hand, in the motoring mode $u_{q,ref}$ should be large enough to counterbalance the q-axis back-EMF and the resistor voltage drop. Thus, one can have the following constraint which is responsible for the maximum reachable speed:

$$u_{q,\min} = R_s i_q + \omega\psi_{m1} \quad (25)$$

Thereby, the permissible range of $u_{q,ref}$ and the reachable speed to the purpose of linear modulation can be represented by the shadowed area in Fig.9. Accordingly, the maximum reachable speed of this faulty drive can be inferred from the intersection of the plots $u_{q,max1}$ and $u_{q,min}$, which is 1085 rpm with $u_{q,ref}$ being 0.853. From the above analysis, the feasible speed range (or input range of $u_{q,ref}$) is remarkably extended in fault mode after applying the proposed transform, which means the attempt to fix this "faulty inverter" is successful.

V. Testing Results

Experiments are conducted on a 4-Pole 5Ph PMSM, which is mechanically coupled to a DC generator. A customized five-phase half-bridge IGBT-based inverter is utilized to feed the 5Ph PMSM, and the drive is loaded via a resistor network connected to the output of the DC generator. A 32-bit floating-point DSP (TMS320F28335) joint with an FPGA (XC3S500E) is developed to execute control algorithms. The PWM generator is programmed in the FPGA, and the control instruction is sent to the FPGA via parallel ports. The DSP's on-chip ADC is triggered by each PWM updating event, and then the DSP core is interrupted on the completion of ADC conversion. The DC bus voltage of the inverter is about 300V, the rotational inertia is about 0.12 kg·m^2, the viscous friction factor is about 0.055 N·m·s, and the switching frequency is 10 kHz. Q of this angular-based RC is 0.93, N is fixed to 175, and a phase-lead up to 2 switching periods is performed to offset the digital delays. For more 5Ph PMSM parameters, refer to Table I. The control system is originally configured with an additional sampling channel for DC bus voltage sensing, and in this work, it is re-configured to sense the faulty phase voltage. This voltage is filtered by an on-board LPF (whose time constant is 0.1ms) prior to sampling. It is worth noting that a considerable phase lag is observed at high speeds which implies the phase-voltage sensing maybe not that reliable as it seems. Thus, this paper is not resorting to the phase-voltage sensing technique to offset the oscillating neutral. As the oscillating neutral is increasingly severe at high speeds, the experiment is conducted at a most reachable high speed in fault mode which is designed to adequately verify the proposed method.

TABLE I
PARAMETERS OF THE PROTOTYPE MOTOR DRIVE

Symbol	Quantity	value
L_d	d-axis inductance	8.32 mH
L_q	q-axis inductance	6.84 mH
L_{d3}	d_3-axis inductance	2.06 mH
L_{q3}	q_3-axis inductance	1.34 mH
ψ_{m1}	the magnitude of 1st rotor flux linkage	0.512 Wb
ψ_{m3}	the magnitude of 3rd rotor flux linkage	0.034 Wb
R_s	phase resistance	1.1 Ω
n_r	the rated speed	1500 rpm

A. Open-loop Methods I, II

Fig.10 shows phase inductances and phase-A back-EMF of the test bench motor. The phase inductances in Fig.10(a) are derived from the finite element analysis of the prototype 5Ph PMSM; whereas the back-EMF in Fig.10(b) is the measured phase-A voltage of 5Ph PMSM in an unloaded case which is dragged by the mechanically coupled DC machine. Take phase-A as an example, the phase-A related inductances comprise not only the self-inductance L_{AA} but also the mutual-inductances, i.e., L_{AB}, L_{AC}, L_{AD}, L_{AE}. Both the self- and mutual inductances are of the same order of magnitude and thus neither of them can be overlooked in fault-tolerant modeling. Besides, phase inductances of the test bench motor are time-variant which are caused by the uneven air gap between the rotor and stator. According to [14], in the presence of phase-A open circuit, the active phase inductances can be

transformed into DCs under a modified Clarke and Park matrices (i.e., (3) and (4) in this work), and the detailed representation of d-q-q_3 frame inductance is referred to [14]. From Fig.10(a) the back-EMF profile of the tested motor is trapezoidal which is originally designed to increase the torque production in normal mode. It has to be noticed that the 5Ph PMSM works in the normal mode for most of its life and it is overtaken by FTC if and only if open faults occur. Unfortunately, according to many literatures, the 3rd harmonic of trapezoidal back-EMF is hazardous to FTC since it introduces torque ripples, and this side-effect can also be explained by (2). It is worth mentioning that the back-EMFs of energized phases also get constant under the new d-q frame proposed by [14]. This work is based on this important study, however, it is found that the simplest SPWM is problematic to fit the formerly developed decoupled model due to ill-consideration of the activity of open-circuited winding, and this paper attempts to fix this defect.

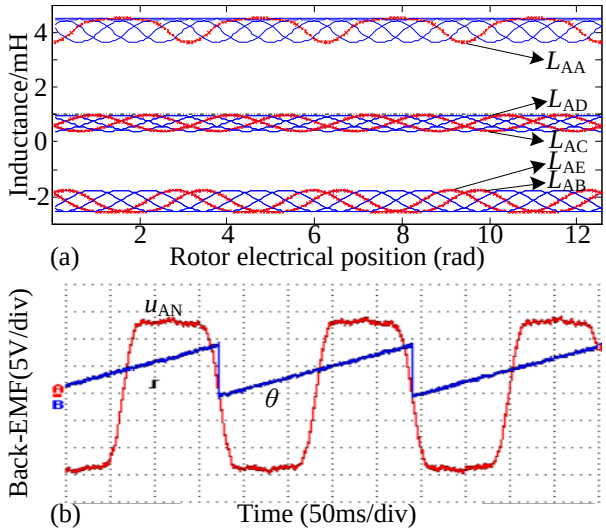

Fig.10 Self- and mutual-inductances as well as the back-EMF of the studied motor. (a) self- and mutual-inductances; (b) the trapezoidal back-EMF.

Fig.11 reveals the back-EMF and phase-A voltage at a relatively lower and higher speed. The faulty phase voltage is of PWM signal and has been smoothed via an on-board LPF. In Fig.11(a) the profile of back-EMF coincides with faulty phase voltage quite well at about 150 rpm. Fig.11(b) refers to the re-constructed back-EMF as well as the phase-to-neutral voltage of phase A at 500 rpm. From Fig.11(b), a substantial 3rd harmonic is present under this speed, and it is explained by the mutually induced EMF caused by the other four energized windings. The deviation between e_A and u_{AN} shows that u_{AN} is indeed affected by the other energized phases. Likewise, it is safe to infer that u_{AN} will conversely influence the active phase voltage generation. At low speeds, the mutual-induced EMFs can be normally neglected. While this mutual-induced EMF is increasingly significant as the motor speed gets higher and higher. Additionally, a slight phase shift between e_A and u_{AN} is observable in Fig.11(b) which is caused by the on-board LPF when filtering u_{AN}, and this is one of the reasons that limit us to resort to the phase-voltage sensing technique. This test illustrates only the back-EMF reconstruction is not enough to overcome the increasingly severe oscillating neutral, and thus some other measurements must be taken.

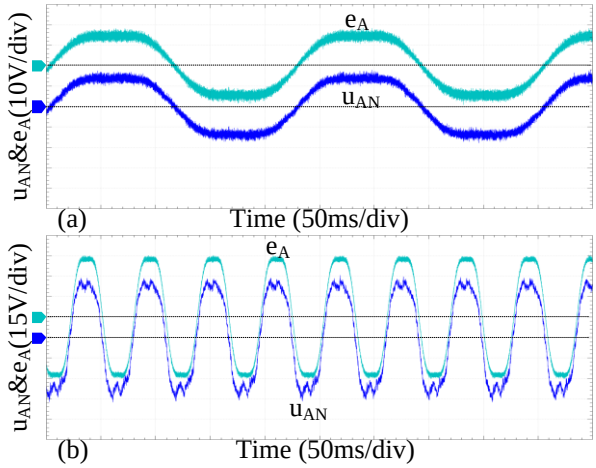

Fig.11 Faulty phase voltage and back-EMF at (a) low speed; and (b) high speed.

Fig.12 shows the d-q frame current at low speeds. In this test, the open-loop control of u_d=0 and u_q=40V is adopted to spin the motor. From Fig.12(a), the d-q frame obviously oscillates at twice the synchronous speed, and the reason for this can be explained by an ill-considered oscillating neutral. In Fig.12(b), the back-EMF, which is assumed identical to the faulty phase voltage at low speeds, is utilized to cancel the impact of oscillating neutral. As it is noticeable that the d-q frame current is quite flat after back-EMF compensation. To sum up, the current profiles agree with the prediction by the decoupled model, and this manifests that the expected phase voltages are generated precisely in the low-speed region. This also indicates that faulty-phase voltage compensation is inevitable to implement the PVM properly.

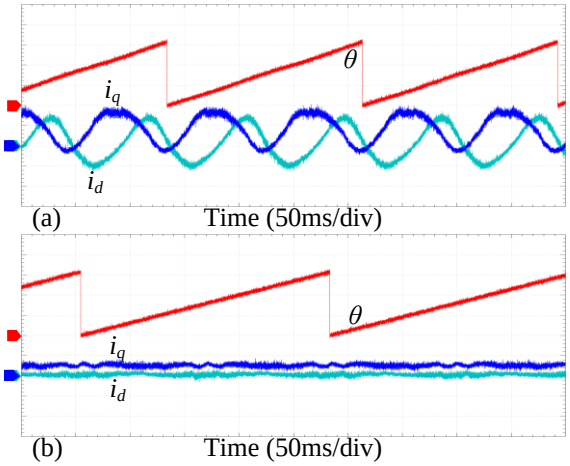

Fig.12 Currents of the d-q frame at low speeds under (a) the SPWM typically for a balanced system; and (b) SPWM with back-EMF compensation. The current is scaled to 5A/div and rotor position is scaled to 200 deg/div.

Fig.13 shows the currents and motor speed at a higher speed under the SPWM with only back-EMF compensation. The open-loop control of u_d=0 and u_q=80V is adopted to spin the motor. From Fig.13(a), the motor is possible to operate steadily at about 500 rpm, and the α-β frame currents are sort of unbalanced, and the d-q frame currents are not that flat as those in the low-speed case. The fluctuation component of d-q frame current can be explained by the remarkable deviation between e_A and u_{AN} at high speeds. In conclusion, some closed-loop methods are required to further suppress these unmodelled mutually induced EMFs.

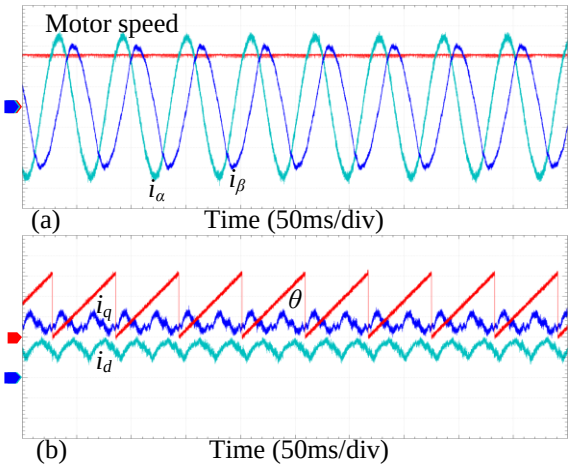

Fig.13 Currents and motor speed at higher speeds under SPWM with back-EMF compensation. (a) α-β frame currents and motor speed; (b) d-q frame currents and rotor position. The current is scaled to 2A/div, rotor position 200 deg/div, motor speed 200 rpm/div.

B. *Closed-loop Methods III, IV*

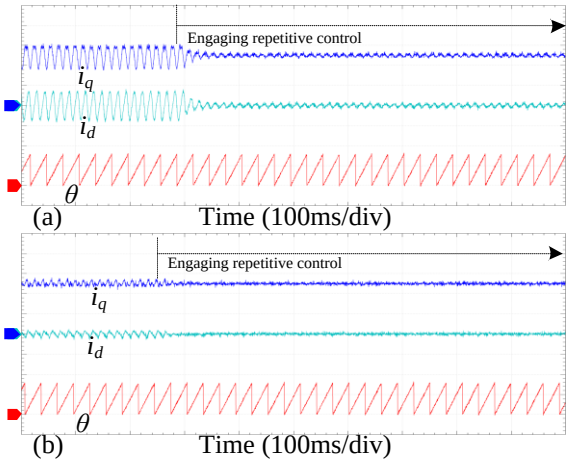

Fig.14 Current performance after engaging the repetitive control under the control of iq=constant. (a) The conventional SPWM with repetitive control; (b) the proposed PVM with back-EMF compensation and repetitive control. The current is scaled to 4A/div and rotor position is scaled to 300 deg/div.

Fig.14 shows the current performance before and after engaging the repetitive control. In this test, the motor is driven under the control of a zero i_d and i_{q3} as well as a constant i_q being 10A. The motor is possible to operate at about 1000 rpm in both two cases. In Fig.14(a), the d-q frame currents have gradually gotten smoother after engaging the repetitive control, however, there still exist visible fluctuations. This confirms the analysis that current harmonics due to oscillating neutral cannot be fully suppressed by merely the repetitive controls. One has to realize that the faulty phase voltage is increasingly remarkable at high speeds, and this implies that the bandwidth of RC shall be quite narrow to fully offset the unmodelled u_{AN}, which, however, could lead the system to the risk of instability. Thus, in a real drive, Q is usually lowered to ensure the control system is with enough stability margin. From Fig.14(b), the current harmonics without an RC are already quite small which are comparable to those in Fig.14(a) using an RC, and this can be explained by fast back-EMF compensation. Thus, the remaining unmodelled mutually induced EMFs, which account for a small proportion of u_{AN}, can be easily suppressed with the RC even at high speeds. Consequently, the effectiveness of the proposed PVM technique can be verified through those comparative experiments.

Fig.15 reveals the performance of this angular based-RC during the speed transient under the proposed PVM. In Fig.15, the motor speed transient is produced by the step change in $i_{q,ref}$ which speeds up the motor from 640rpm to about 1000 rpm. This step command is aimed to emulate aperiodic disturbances so as to examine the robustness of the RC with respect to speed variation. Evidently, the faulty drive transitions smoothly and d-q-q_3 frame currents are fully under control, which confirms the validity of the angular-based RC in adjustable speed drives.

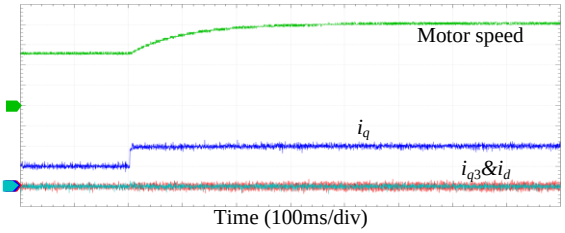

Fig.15 The performance of this angular based-RC during the speed transient under the proposed PVM. The currents are scaled to 5A/div and motor speed is scaled to 250 rpm/div.

C. *FTC test* (*Torque ripple reduction*)

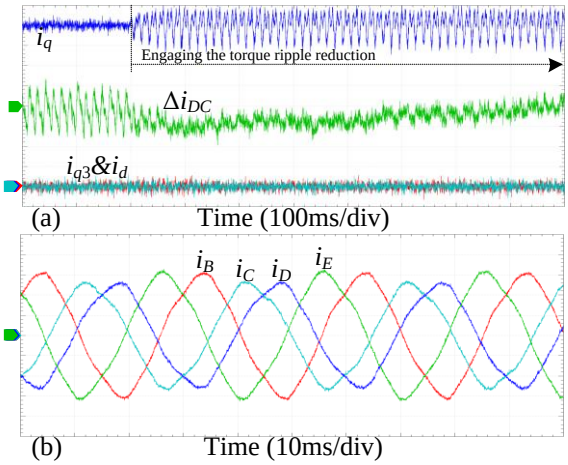

Fig.16 Torque ripple reduction performance basing on the proposed PVM scheme. (a) d-q-q3 frame currents and Δi_{DC}; (b) remaining phase currents. The d-q-q3 frame currents are scaled to 1.25A/div, the phase currents are scaled to 5A/div. and Δi_{DC} is scaled to 0.05A/div.

Fig.16 shows the FTC test, which is aimed to reduce torque ripples basing on the proposed PVM scheme. The optimal current for this purpose is referred to as A(3) which comprises 2nd, 4th, and 6th harmonics, and the DC bus voltage is also temporarily increased to 335V for the purpose of harmonic control during the torque ripple reduction. Encouragingly, the adopted RC is still sufficient in tracking these AC references. In this work, the output current of shaft coupled DC generator, i_{DC}, is measured and zoomed-in to demonstrate the torque ripple behavior. From Fig.16(a), the q-axis current follows its reference after engaging FTC, and simultaneously Δi_{DC} starts to fade away which provides strong evidence that torque ripple reduction is achieved. The oscillation amplitude (peak-to-peak) accounts for about 0.2% of i_{DC} under FTC, and the remaining ripples in i_{DC} are probably caused by the misaligned shaft, cogging torque as well as the unmodelled constituent. The waveforms of phase currents under this FTC are presented in Fig.16(b) and they coincide with their corresponding references

which can be easily obtained by the inverse Park and Clarke transforms of the $i_{q,ref}$ in A(3) that dedicated to the FTC purpose. This test illustrates that the FTC currents are likewise controllable under the proposed PVM.

VI. Conclusion

The phase voltage modulation (PVM) suffers from neutral oscillation under open faults, and thus the previous fault-tolerant FOC, which is dedicated to a more generic 5Ph PMSM, performs improperly. To this end, a nonlinear transform incorporating faulty phase voltage is worked out theoretically, and several approaches to cancel the need for voltage sensors are comparatively studied. Consequently, an angular-based repetitive control joint with back-EMF compensation is proposed which redefines pole voltages so as to enhance the controllability of the phase voltage/current, and its superiority is well confirmed by the experimental results.

Appendix

According to (1) and (2), The minimum joule losses (MJL) and the corresponding torque, in this case, can be given by:

$$MJL = R\left(i_d^2 + i_q^2 + i_{q3}^2\right)\Big|_{i_d=0, i_{q3}=0} = Ri_q^2 \tag{A1}$$

$$T_e\Big|_{i_d=0, i_{q3}=0} = 2.5p\psi_{m1}i_q\left[1+\frac{1.5\psi_{m3}\left(-\cos 2\theta+\cos 4\theta\right)}{\psi_{m1}}\right] \tag{A2}$$

Thus, the optimal current solution for torque ripple-free can be represented by

$$i_{q,ref} = \frac{T_{e,ref}}{2.5p\psi_{m1}}\frac{\psi_{m1}}{\left[\psi_{m1}+1.5\psi_{m3}\left(-\cos 2\theta+\cos 4\theta\right)\right]} \tag{A3}$$

References

[1] A. Arafat, S. Choi, and J. Baek, "Open-Phase Fault Detection of a Five-Phase Permanent Magnet Assisted Synchronous Reluctance Motor Based on Symmetrical Components Theory," *IEEE Transactions on Industrial Electronics*, vol. 64, no. 8, pp. 6465-6474, 2017.

[2] Y. Zeng, M. Cheng, G. Liu, and W. Zhao, "Effects of Magnet Shape on Torque Capability of Surface-mounted Permanent Magnet Machine for Servo Applications," *IEEE Transactions on Industrial Electronics*, pp. 1-1, 2019.

[3] A. Mohammadpour and L. Parsa, "Global Fault-Tolerant Control Technique for Multiphase Permanent-Magnet Machines," *IEEE Transactions on Industry Applications*, vol. 51, no. 1, pp. 178-186, 2015.

[4] H. Guzman *et al.*, "Comparative Study of Predictive and Resonant Controllers in Fault-Tolerant Five-Phase Induction Motor Drives," *IEEE Transactions on Industrial Electronics*, vol. 63, no. 1, pp. 606-617, 2016.

[5] E. B. Sedrine, J. Ojeda, M. Gabsi, and I. Slama-Belkhodja, "Fault-Tolerant Control Using the GA Optimization Considering the Reluctance Torque of a Five-Phase Flux Switching Machine," *IEEE Transactions on Energy Conversion*, vol. 30, no. 3, pp. 927-938, 2015.

[6] H. Zhou, W. Zhao, G. Liu, R. Cheng, and Y. Xie, "Remedial Field-Oriented Control of Five-Phase Fault-Tolerant Permanent-Magnet Motor by Using Reduced-Order Transformation Matrices," *IEEE Transactions on Industrial Electronics*, vol. 64, no. 1, pp. 169-178, 2017.

[7] W. Huang, W. Hua, F. Chen, F. Yin, and J. Qi, "Model Predictive Current Control of Open-Circuit Fault-Tolerant Five-Phase Flux-Switching Permanent Magnet Motor Drives," *IEEE Journal of Emerging and Selected Topics in Power Electronics*, vol. 6, no. 4, pp. 1840-1849, 2018.

[8] G. Liu, Z. Lin, W. Zhao, Q. Chen, and G. Xu, "Third Harmonic Current Injection in Fault-Tolerant Five-Phase Permanent-Magnet Motor Drive," *IEEE Transactions on Power Electronics*, vol. 33, no. 8, pp. 6970-6979, 2018.

[9] R. Cui, Y. Fan, and M. Cheng, "A New Zero-Sequence Current Suppression Control Strategy for Five-Phase Open-Winding Fault-tolerant Fractional-slot Concentrated Winding IPM Motor Driving System," *IEEE Transactions on Industry Applications*, pp. 1-1, 2019.

[10] B. Tian, Q. An, J. Duan, D. Semenov, D. Sun, and L. Sun, "Cancellation of Torque Ripples With FOC Strategy Under Two-Phase Failures of the Five-Phase PM Motor," *IEEE Transactions on Power Electronics*, vol. 32, no. 7, pp. 5459-5472, 2017.

[11] Y. Sui, P. Zheng, Z. Yin, M. Wang, and C. Wang, "Open-Circuit Fault-Tolerant Control of Five-Phase PM Machine Based on Reconfiguring Maximum Round Magnetomotive Force," *IEEE Transactions on Industrial Electronics*, vol. 66, no. 1, pp. 48-59, 2019.

[12] G. Liu, L. Qu, W. Zhao, Q. Chen, and Y. Xie, "Comparison of Two SVPWM Control Strategies of Five-Phase Fault-Tolerant Permanent-Magnet Motor," *IEEE Transactions on Power Electronics*, vol. 31, no. 9, pp. 6621-6630, 2016.

[13] Q. Chen, G. Liu, W. Zhao, L. Qu, and G. Xu, "Asymmetrical SVPWM Fault-Tolerant Control of Five-Phase PM Brushless Motors," *IEEE Transactions on Energy Conversion*, vol. 32, no. 1, pp. 12-22, 2017.

[14] B. Tian, Q. An, J. Duan, D. Sun, L. Sun, and D. Semenov, "Decoupled Modeling and Nonlinear Speed Control for Five-Phase PM Motor Under Single-Phase Open Fault," *IEEE Transactions on Power Electronics*, vol. 32, no. 7, pp. 5473-5486, 2017.

[15] L. Cheng, Y. Sui, P. Zheng, P. Wang, and F. Wu, "Implementation of Postfault Decoupling Vector Control and Mitigation of Current Ripple for Five-Phase Fault-Tolerant PM Machine Under Single-Phase Open-Circuit Fault," *IEEE Transactions on Power Electronics*, vol. 33, no. 10, pp. 8623-8636, 2018.

[16] A. K. M. Arafat and S. Choi, "Optimal Phase Advance Under Fault-Tolerant Control of a Five-Phase Permanent Magnet Assisted Synchronous Reluctance Motor," *IEEE Transactions on Industrial Electronics*, vol. 65, no. 4, pp. 2915-2924, 2018.

[17] M. Bermudez, I. Gonzalez-Prieto, F. Barrero, H. Guzman, X. Kestelyn, and M. J. Duran, "An Experimental Assessment of Open-Phase Fault-Tolerant Virtual-Vector-Based Direct Torque Control in Five-Phase Induction Motor Drives," *IEEE Transactions on Power Electronics*, vol. 33, no. 3, pp. 2774-2784, 2018.

[18] B. Tian, G. Mirzaeva, Q. An, L. Sun, and D. Semenov, "Fault-Tolerant Control of a Five-Phase Permanent Magnet Synchronous Motor for Industry Applications," *IEEE Transactions on Industry Applications*, vol. 54, no. 4, pp. 3943-3952, 2018.

[19] L. Zhang, Y. Fan, R. Cui, R. D. Lorenz, and M. Cheng, "Fault-Tolerant Direct Torque Control of Five-Phase FTFSCW-IPM Motor Based on Analogous Three-Phase SVPWM for Electric Vehicle Applications," *IEEE Transactions on Vehicular Technology*, vol. 67, no. 2, pp. 910-919, 2018.

[20] M. Priestley, M. Farshadnia, and J. Fletcher, "FOC Transformation for Single Open-Phase Faults in the Five-Phase Open-End Winding Topology," *IEEE Transactions on Industrial Electronics*, pp. 1-1, 2019.

[21] H. Guzman, F. Barrero, and M. J. Duran, "IGBT-Gating Failure Effect on a Fault-Tolerant Predictive Current-Controlled Five-Phase Induction Motor Drive," *IEEE Transactions on Industrial Electronics*, vol. 62, no. 1, pp. 15-20, 2015.

[22] M. J. Durán, J. Prieto, F. Barrero, J. A. Riveros, and H. Guzman, "Space-Vector PWM With Reduced Common-Mode Voltage for Five-Phase Induction Motor Drives," *IEEE Transactions on Industrial Electronics*, vol. 60, no. 10, pp. 4159-4168, 2013.

[23] S. M. Dabour, A. S. Abdel-Khalik, A. M. Massoud, and S. Ahmed, "Analysis of Scalar PWM Approach With Optimal Common-Mode Voltage Reduction Technique for Five-Phase Inverters," *IEEE Journal of Emerging and Selected Topics in Power Electronics*, vol. 7, no. 3, pp. 1854-1871, 2019.

[24] H. Tian, P. Y. Li, and J. D. V. d. Ven, "Valve Timing Control for a Digital Displacement Hydraulic Motor Using an Angle-Domain Repetitive Controller," *IEEE/ASME Transactions on Mechatronics*, vol. 24, no. 3, pp. 1306-1315, 2019.

[25] M. Tang, A. Gaeta, A. Formentini, and P. Zanchetta, "A Fractional Delay Variable Frequency Repetitive Control for Torque Ripple Reduction in PMSMs," *IEEE Transactions on Industry Applications*, vol. 53, no. 6, pp. 5553-5562, 2017.

[26] Q. Zhao and Y. Ye, "A PIMR-Type Repetitive Control for a Grid-Tied Inverter: Structure, Analysis, and Design," *IEEE Transactions on Power Electronics*, vol. 33, no. 3, pp. 2730-2739, 2018.

Bing Tian received the B.S. and M.S. degrees in electrical engineering from Harbin Engineering University, Harbin, China, in 2011 and 2013, respectively; and Ph.D. degree in electrical engineering from Harbin Institute of Technology, Harbin, China, in 2018. From 2018 to 2020, He was a research fellow with Norwegian University of Science and Technology (NTNU), Trondheim, Norway, working on the electrification of offshore production system in close collaboration with Norwegian industry. Since September 2020, he has been a Research Associate Professor with the department of electrical engineering of Nanjing University of Aeronautics and Astronautics (NUAA), Nanjing, China. His current research interests include fault-tolerant control of multi-phase drives, sensorless control of electric drives, neural network, sliding mode controller/observer, and repetitive control.

Li Sun (M'08) received the B.S., M.S. and Ph. D. degrees in electrical engineering from Harbin Institute of Technology, Harbin, China, in 1982, 1986 and 1991, respectively. Since 1986, he has been with Department of Electrical Engineering, Harbin Institute of Technology, where he is currently a Professor in Electrical Engineering. His research interests include electric machines and drives, renewable energy, power electronics, and EMC.

Marta Molinas (M'94) received the Diploma degree in electromechanical engineering from the National University of Asuncion, Asuncion, Paraguay, in 1992; the Master of Engineering degree from Ryukyu University, Japan, in 1997; and the Doctor of Engineering degree from the Tokyo Institute of Technology, Tokyo, Japan, in 2000. She was a Guest Researcher with the University of Padova, Padova, Italy, during 1998. From 2004 to 2007, she was a Postdoctoral Researcher with the Norwegian University of Science and Technology (NTNU) and from 2008-2014 she has been professor at the Department of Electric Power Engineering at the same university. She is currently Professor at the Department of Engineering Cybernetics, NTNU. Her research interests include stability of power electronics systems, harmonics, instantaneous frequency, and non-stationary signals from the human and the machine. She is Associate Editor for the IEEE Journal JESTPE, IEEE PELS Transactions and Editor of the IEEE Transactions on Energy Conversion. Dr. Molinas has been an AdCom Member of the IEEE Power Electronics Society from 2009 to 2011.

Qun-Tao An (S'10–M'11) received the B.S. degree in electrical engineering from Harbin University of Science and Technology, Harbin, China, in 2004, and the M.S. and Ph.D. degrees in electrical engineering from Harbin Institute of Technology, Harbin, China, in 2006 and 2011, respectively. From 2009 to 2010, he was an honorary fellow at Wisconsin Electric Machines and Power Electronics Consortium, University of Wisconsin-Madison. From 2009, he joined the faculty of Harbin Institute of Technology, and he is currently an Associate Professor. His research interests include electric machines and drives, power electronics, and energy storage technology.